AGU PUBLICATIONS

JGR

Journal of Geophysical Research: Space Physics

RESEARCH ARTICLE
10.1002/2017JA024809

Key Points:
- Enhanced plasma line and ion lines were observed by UHF ISR within the extending altitude range, where Bragg condition should be satisfied
- Within the altitude range, electron temperature and ion mass compensate each other so that ion acoustic wave satisfies Bragg condition
- For a small gradient profile of density, temperature and density compensate each other so that Langmuir wave satisfies Bragg condition

Correspondence to:
J. Wu,
wujun1969@163.com

Citation:
Wu, J., Wu, J., Rietveld, M. T., Haggstrom, I., Xu, Z., & Zhao, H. (2018). The extending of observing altitudes of plasma and ion lines during ionospheric heating. *Journal of Geophysical Research: Space Physics*, *123*, 918–930. https://doi.org/10.1002/2017JA024809

Received 25 SEP 2017
Accepted 5 JAN 2018
Accepted article online 16 JAN 2018
Published online 26 JAN 2018

The Extending of Observing Altitudes of Plasma and Ion Lines During Ionospheric Heating

Jun Wu[1], Jian Wu[1], M. T. Rietveld[2,3], I. Haggstrom[4], Zhengwen Xu[1], and Haisheng Zhao[1]

[1]National Key Laboratory of Electromagnetic Environment, China Research Institute of Radio Wave Propagation, Beijing, China, [2]EISCAT, Tromsø, Norway, [3]Department of Physics, UiT, The Arctic University of Norway, Tromsø, Norway, [4]EISCAT Scientific Association, Kiruna, Sweden

Abstract The ultrahigh-frequency observation during an ionospheric heating experiment on 11 March 2014 at the European Incoherent Scatter Scientific Association Tromsø site illustrated a remarkable extension of observing altitudes of the enhanced plasma line and the ion line, implying that the enhanced ion acoustic wave and Langmuir wave should satisfy the Bragg condition within the extending altitude range. An analysis shows that the dependence of the wave number of the traveling ion acoustic wave on the profiles of enhanced electron temperature and ion mass, as are expected from the dispersion relation of the ion acoustic wave, leads to the extension of observing altitudes of the enhanced ion line. In addition, the altitude extension of the enhanced plasma line is dependent mainly on the profile of the electron density, although it is not independent of the profile of the electron temperature. Considering a small gradient profile of electron density, however, the enhanced electron temperature, as well as the thermal conduction along the magnetic field, may lead to the altitude extension of the enhanced plasma line.

1. Introduction

Only temperature and density modifications were originally intended in early ionospheric heating experiments, but a much greater variety of physical phenomena have been observed. One of the most interesting of these physical phenomena is the enhanced plasma line and the ion line observed by incoherent scatter radar (ISR).

The pump-enhanced plasma line and ion line can be interpreted by parametric decay instability (PDI) and oscillating two-stream instability (OTSI) (Stubbe et al., 1992), which has been studied extensively (Chen & Fejer, 1975; DuBois & Goldman, 1965, 1967; Drake et al., 1974; Fejer, 1979; Kohl et al., 1993; Kuo & Cheo, 1978; Kuo & Fejer, 1972; Perkins & Flick, 1971; Perkins et al., 1974; Rosenbluth, 1972; Silin, 1965; Stubbe et al., 1992; Wu et al., 2006, 2007). Based on some measurements obtained by ISR during ionospheric heating experiments, the structure of the ISR spectrum (Carlson et al., 1972; Dubois et al., 1988; Gordon & Carlson, 1974; Hagfors et al., 1983; Kantor, 1974; Kohl et al., 1993; Kuo & Fejer, 1972; Nordling et al., 1988; Stubbe et al., 1985, 1992), the threshold to excite PDI and OTSI (Bezzerides & Weinstock, 1972; Dubois & Goldman, 1972; Perkins et al., 1974; Weinstock & Bezzerides, 1972), and the characteristic time of PDI and OTSI (Carlson et al., 1972; Gordon & Carlson, 1974; Jones et al., 1986; Kantor, 1974; Kohl et al., 1993; Stubbe et al., 1985) have been investigated. Additionally, PDI and OTSI can be excited by the O-mode pump (Carlson et al., 1972; Kantor, 1974) and by the X-mode pump (Blagoveshchenskaya et al., 2014).

Based on the Zakharov model, DuBois et al. (1988) developed a new theoretical approach called strong Langmuir turbulence (SLT), which has led to new insights into the enhanced plasma line and ion line induced by ionospheric heating. The ISR spectrum induced by SLT contains a caviton continuum plus a free mode in the plasma line spectrum and a zero-frequency feature in the ion line spectrum (Cheung et al., 1992, 2001; Dubois et al., 1988, 1990, 1993a, 1993b, 2001). SLT can be excited by the pump slightly above the threshold for PDI in the region very close to the reflection altitude of the pump (Cheung et al., 2001; Dubois et al., 1990, 1993a, 2001). For ionospheric parameters, PDI and SLT may coexist (Djuth & Dubois, 2015; Dubois et al., 1988, 1990, 1991). PDI may play a role in the first few milliseconds following the pump onset, whereas the Langmuir turbulence is sustained by SLT after PDI (Djuth & Dubois, 2015; Dubois et al., 1988, 1990, 1991).

However, no well-grounded theoretical model can comprehensively explain the enhanced plasma line and ion line and be accepted universally. Stubbe et al. (1992) claim that the propagating Langmuir and ion

acoustic waves represent the major features and parametric decay represents the major process within the field of Langmuir turbulence, whereas Cheung et al. (1992, 2001), Dubois et al. (1990, 1993a, 1993b), and Kohl et al. (1993) support the theory that SLT can interpret those observations obtained by ISR more reasonably, and PDI and SLT may coexist.

Usually, the pump-enhanced Langmuir wave and ion acoustic wave are induced by PDI and OTSI in the altitude range extending from the reflection altitude of the pump downward to altitudes where resonant Langmuir waves having large wave numbers are heavily Landau-damped (Stubbe et al., 1992). The width of the excitation range is 0.1*H*, where *H* is the scale height of the ionosphere plasma (Stubbe et al., 1992). The enhanced Langmuir wave and ion acoustic wave traveling downward can be observed by radar at the altitude where the Bragg condition is satisfied (Kohl et al., 1987, 1993; Stubbe et al., 1992). Stubbe et al. (1992) and Kohl et al. (1993) presented an altitude profile of the normalized ion line power, which showed the extending altitude of ~3 km to 5 km. This profile is always valid at the European Incoherent Scatter Scientific Association (EISCAT) UHF radar, but it is difficult to explain. Stubbe et al. (1992) and Kohl et al. (1993) thought the profile was due to the virtual observation at a frequency of 933 MHz/2. Djuth et al. (1994) also reported some observations obtained at EISCAT that the plasma turbulence plunged downward and extended in altitude over timescales of tens of seconds after the pump went on and suggested that this phenomenon was most likely caused by the change in the electron density profile brought about by the heating of the ionospheric plasma. The EISCAT UHF radar observed a persistent enhancement in ion line induced by an O-mode pump at a frequency of 5.423 MHz, which started at ~230 km and descended to ~220 km within ~60 s in the heating period (Ashrafi et al., 2006). Ashrafi et al. (2006) suggested that the clear descent in the altitude of the enhanced ion line represented the change in electron density during heating. The EISCAT very high frequency (VHF) data also showed the descent in altitude of the enhanced ion line and plasma line during heating, which was also attributed to the variety of profiles of electron density induced by heating in the vicinity of the reflection altitude (Cheng et al., 2013). In addition, Wang et al. (2016) presented an experimental observation that showed the extending altitude of the enhanced ion line, which was attributed to PDI excited by the pump in the X mode.

In this paper, particular attention is not paid to the excitation of the enhanced plasma line and ion line but rather to the altitude extension of the enhanced ion line and plasma line, and a new explanation responsible for the phenomenon is given.

2. Experiment and Data

The ionospheric heating campaign reported here was carried out at 12:32:30 UT–14:30 UT (universal time) on 11 March 2014 at the EISCAT site near Tromsø in northern Norway (69.58°N, 19.21°E, magnetic dip angle I = 78°). The experiment involved the EISCAT heater (Rietveld et al., 1993, 2016) used to modify the *F* region of the ionosphere and EISCAT UHF ISR (Rishbeth & Van Eyken, 1993) as the principal means of diagnosis. A detailed description of the experimental arrangement has been given by Wu, Wu, and Xu (2016) and Wu et al. (2017). In short, the O-mode pump frequency was operated from 6.7 MHz to 7 MHz and changed in a step of 2.804 kHz with a period of 10 s, as shown in Figures 1 and 2 (seventh panels) and 3 (bottom). The effective radiated power of the pump was calculated to be in the range of 56 MW–78 MW; that is, the electric field at an altitude ~200 km should be in the range of 0.3 V/m–0.35 V/m (Rietveld et al., 1993), which can satisfy the threshold (~0.1 V/m) of PDI for the typical *F* region ionosphere (Robinson, 1989). Moreover, the beam of the EISCAT heater and the UHF ISR were directed to field alignment (actually 12° south of the zenith).

The ionospheric and geomagnetic conditions were relatively inactive during the experiment. The total magnetic strength at altitude 200 km varied in the interval of [49,210 nT, 49,240 nT], which was obtained by extrapolating the total magnetic data provided by Tromsø Geophysical Observatory, UiT, The Arctic University of Norway, where "[ ]" is the closed interval. Correspondingly, the fifth electron gyroharmonic at altitude 200 km is in the interval of [6.8922 MHz, 6.8964 MHz], which lies in the interval of pump frequency f_{HF} [6.7 MHz, 7 MHz] exactly. Moreover, the measurement of the Dynasonde at EISCAT showed that the mean critical plasma frequency of the ionosphere was ~9 MHz at the F_2 cutoff altitude of ~280 km from 12:30 UT to 14:00 UT and decreased to ~8.54 MHz from 14:00 UT to 14:30 UT.

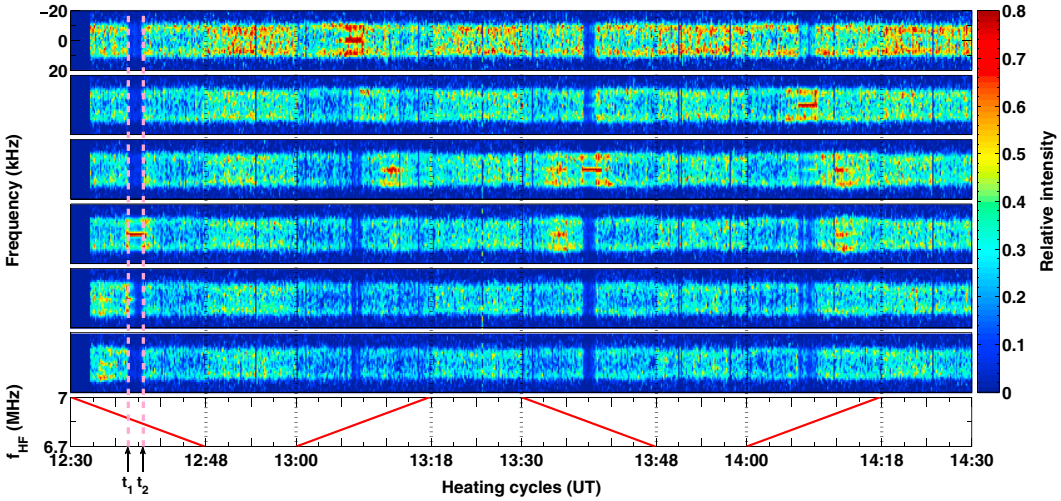

Figure 1. The ion lines at altitudes of (first panel) 215.43 km, (second panel) 212.5 km, (third panel) 209.57 km, (fourth panel) 206.63 km, (fifth panel) 203.7 km, and (sixth panel) 200.77 km versus (seventh panel) heating cycles.

In addition, to measure the effect induced by the pump for each step of frequency, the radar data were analyzed using an integration time of 10 s by version 8.7 of Grand Unified Incoherent Scatter Design and Analysis Package (Lehtinen & Huuskonen, 1996) and version 2.67 of Real Time Graphic provided by EISCAT.

To facilitate the following description and discussion, it is necessary to give the convention of the division of f_{HF}: the pump frequency band of [6.7 MHz, 7 MHz] can be divided into three bands according to the dependence of the ion line on f_{HF} shown in Figure 1, namely, the higher band (HB, above $5f_{ce}$, where f_{ce} is the local electron gyrofrequency at altitude ~200 km with a value of ~1.366 MHz in Tromsø), the gyroharmonic band (GB, close to $5f_{ce}$), and the lower band (LB, below $5f_{ce}$). For instance, we choose the HB to be **(**6.871028 MHz, 7 MHz], the GB to be [6.837383 MHz, 6.871028 MHz], and the LB to be [6.7 MHz, 6.837383 MHz**)** in the first cycle, which are marked with [12:30:00 UT, t_1**)**, [t_1, t_2] and **(**t_2, 12:48:00 UT]**,** respectively, as indicated on the abscissa in Figures 1, 2, and 3 where t_1 denotes 12:37:40 UT, t_2 12:39:40 UT, "( )" the open interval and "[ ]" the closed interval. Here it should be stressed that due to the slight variation of the geomagnetic field, $5f_{ce}$ was not a constant but varied slightly. Thus, the above division in each cycle should be slightly different.

In Figure 1 (first to sixth panels), the ion lines within the interval of [−20 kHz, 20 kHz] at altitudes of 215.43 km, 212.5 km, 209.57 km, 206.63 km, 203.7 km, and 200.77 km, respectively, are given. When f_{HF} lies in the GB, the

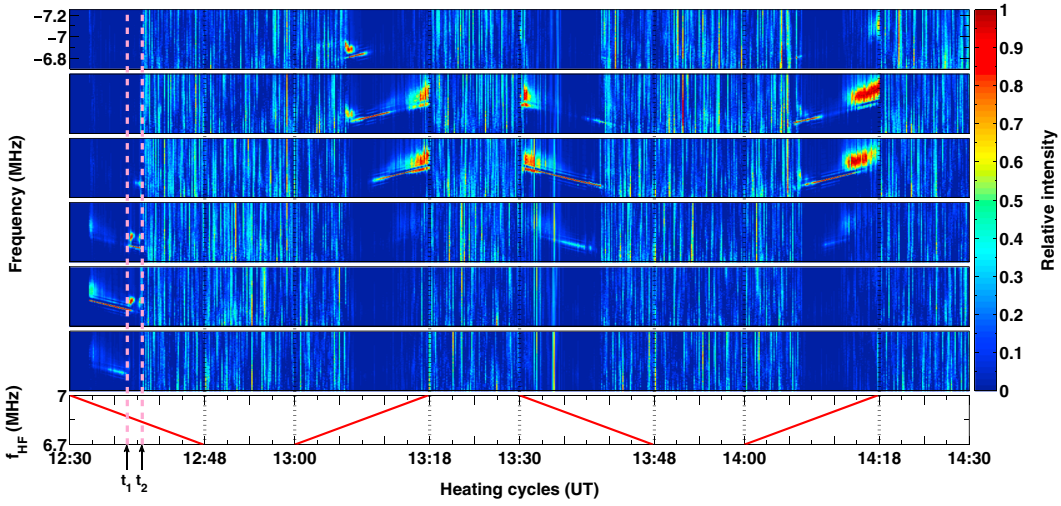

Figure 2. The plasma line at altitudes of (first panel) 210.25 km, (second panel) 207.32 km, (third panel) 204.39 km, (fourth panel) 201.45 km, (fifth panel) 198.52 km, and (sixth panel) 195.58 km versus (seventh panel) heating cycles.

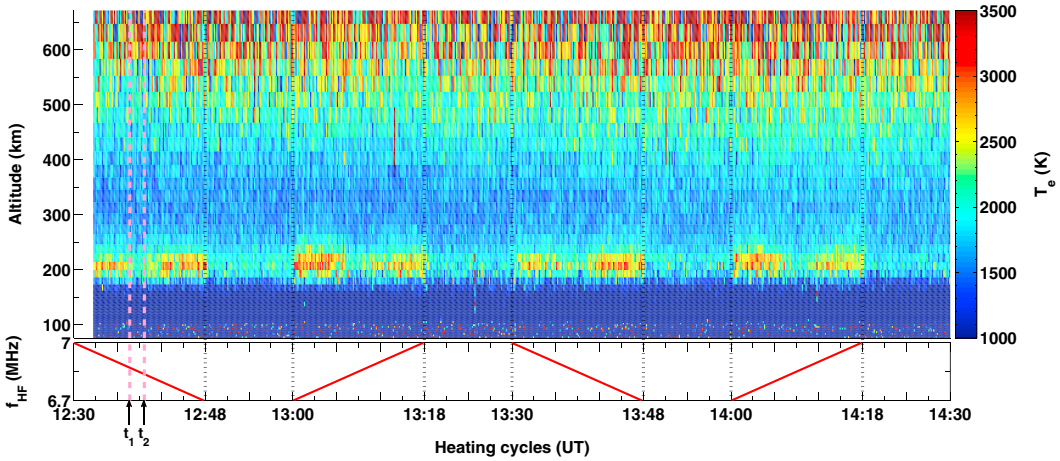

Figure 3. The electron temperature T_e versus heating cycles.

enhanced ion line reaches ~1 and occurs at altitudes of 206.63 km in the first heating cycle (12:30 UT–12:48 UT), 215.43 km in the second heating cycle (13:00 UT–13:18 UT), 209.57 km in the third heating cycle (13:30 UT–13:48 UT), and 212.5 km in the fourth heating cycle (14:00 UT–14:18 UT). At other altitudes, however, some gaps or weak ion line spectra appear, which are caused by the normalization to the strongest value of the ion line at any specific time and altitude and do not imply a real decrease in the ion line or any unusual response.

When f_{HF} steps in the HB, the enhanced ion line of up to ~0.85 occurs at a lower altitude than in the GB and is distributed within a remarkably wide altitude range, for instance, at altitudes of 209.57 km and 206.63 km in the fourth heating cycle. Moreover, two prominent features shared in the HB and GB are the significant "spikes" in the center of the ion line spectra, which are the manifestation of the oscillating two-stream instability (OTSI) or the purely growing instability and the significant "shoulders" lying at a frequency of ~9.45 kHz, which is the confirmation of the parametric decay instability (PDI) (Kohl et al., 1993; Stubbe et al., 1992).

When f_{HF} is in the LB, the ion line shows a decrease in intensity instead of an enhancement. Namely, no significant "spikes" and "shoulders" are found in those ion lines. The mechanism responsible for the decrease in the ion line in the LB is beyond the scope of this paper.

Usually, the altitude of the plasma line is approximately 3 km–5 km lower than the altitude of the ion line at EISCAT UHF (Kohl et al., 1993; Stubbe et al., 1992). Accordingly, the downshifted plasma lines within the frequency range of [−6.7 MHz, −7.25 MHz] at altitudes of 210.25 km, 207.32 km, 204.39 km, 201.45 km, 198.52 km, and 195.58 km are illustrated successively from Figure 2 (first to sixth panels). One can find the distribution of the altitude of the enhanced plasma line as analogous to the distribution of the altitude of the enhanced ion line. In the GB, some strong enhanced plasma lines reach ~1 and are located at altitudes of 204.39 km, 201.45 km, and 198.52 km in the first heating cycle; 210.25 km and 207.32 km in the second heating cycle, and 207.32 km and 204.39 km in the third and fourth cycles. In the HB, however, those enhanced plasma lines plunge downward in altitude and are located at altitudes of 201.45 km, 198.52 km, and 195.58 km in the first heating cycle; 207.32 km and 204.39 km in the second heating cycle; and 207.32 km, 204.39 km, and 201.45 km in the third and fourth cycles. In the LB, the enhancement in the plasma line has not been found at any of those altitudes. In a way similar to the ion line, these plasma lines show similar weakening intervals caused by the normalization, but they occur in the GB and HB.

At those altitudes, there are two "bands" of plasma lines in the HB and GB, the lower one of which lies at frequency $f_{HF} - f_{ia}$, as is expected for a "decay line" from PDI excited by the pump, where f_{ia} is the frequency of ion acoustic wave and ~9.45 kHz here, and the upper one of which is the spread of the plasma lines and occurs only at higher frequencies of (~6.93 MHz to ~7.15 MHz). Some possible explanations of the upper "band" of plasma lines, such as the interaction of four plasma waves (Borisova et al., 2016), the inhomogeneous increase in electron density by irregularities induced by the pump (Wu et al., 2016), and the free Langmuir wave excited by SLT (Dubois et al., 1988, 1990, 1991, 1993a, 1993b), were given (Wu et al., 2017), but the nature of the upper "band" of plasma lines still remains open.

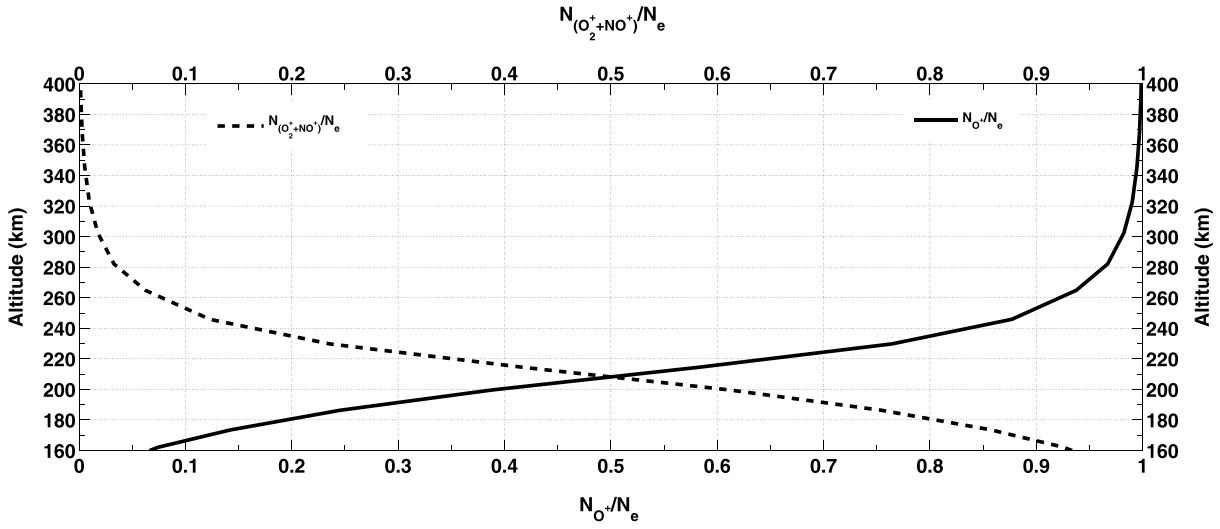

Figure 4. The ratios of N_{O^+} and $N_{(O_2^+ + NO^+)}$ to N_e, respectively, as an altitude function.

Figure 3 gives the altitude profile of electron temperature T_e with the height resolution of 13 km–19 km as a function of the heating cycle. Near an altitude of ~200 km, the enhancement in T_e is evidently a function of f_{HF}, that is, $T_{eLB200} > T_{eHB200} > T_{eGB200}$, where T_{eLB200}, T_{eHB200}, and T_{eGB200} are the electron temperatures in the LB, HB, and GB, respectively, near an altitude of ~200 km. The means of T_{eLB200}, T_{eHB200}, and T_{eGB200} are ~2,782 K, ~2,687 K, and ~2,268 K in the first heating cycle; ~2,882 K, ~2,505 K, and ~2,103 K in the second heating cycle; ~2,815 K, ~2,581 K, and ~2,348 K in the third heating cycle; and ~2,667 K, ~2,599 K, and ~2,186 K in the fourth heating cycle. This change in T_e with f_{HF} is dependent on the dispersion behavior of the electrostatic upper hybrid waves excited by an O-mode pump lying in the GB, HB, and LB (Borisova et al., 2014, 2016; Dysthe et al., 1982; Gurevich et al., 1995; Mjølhus, 1993; Robinson et al., 1996; Wu et al., 2017). In general, the upper hybrid resonance altitude of the pump is approximately 2 km–10 km lower than the reflection altitude of the pump, which is dependent on the altitude profile of the ionospheric electron density (Gurevich, 2007).

Figure 4 illustrates the ratio of the oxygen ion density N_{O^+} to the electron density N_e and the ratio of the nitric oxide ion plus molecular oxygen ion density $N_{(O_2^+ + NO^+)}$ to the electron density N_e as a function of altitude, which is given by International Reference Ionosphere 2007 (IRI-2007) model (Bilitza & Reinisch, 2008) and is invoked by the version 8.7 of Grand Unified Incoherent Scatter Design and Analysis Package (Lehtinen & Huuskonen, 1996). Note that the mass of O_2^+ is approximately equal to the mass of NO^+; thus, O_2^+ and NO^+ are considered in the combining way. Moreover, for the sake of simplicity, only O^+, O_2^+, and NO^+ are considered, whereas hydrogen ion H^+, atomic nitrogen ion N^+, and helium ion H_e^+ are ignored due to the small mass or the small percentage. Indeed, the frequency of the ion acoustic wave mode corresponding to H^+ $f_{iaH^+} = \frac{2k_r}{2\pi}\sqrt{\gamma\frac{K_B T_e}{m_{iH^+}}} \approx 46$kHz, which is excluded in the ion line channel of [− 40 kHz, 40 kHz] of UHF radar, where k_r is the wave number of UHF radar, γ is the adiabatic index, K_B is the Boltzmann constant, m_{iH^+} is the mass of H^+, and T_e is set as the 2,186 K, namely, T_{eGB200} in the fourth heating cycle. In other words, the ion acoustic wave mode corresponding to H^+ cannot be observed by the UHF radar. Similarly, the frequencies of the ion acoustic wave modes corresponding to N^+ and H_e^+ are ~12.2 kHz and ~22.8 kHz, respectively, which deviate greatly from the examined frequency of the enhanced ion line ~9.45 kHz. Additionally, in the examined altitude range of 200.77 km to 215.43 km, the percentages of H^+, N^+, and H_e^+ are so small that they cannot be given by IRI-2007. Figure 4 obviously shows that $\frac{N_{O^+}}{N_e}$ descends monotonically with the descent in the altitude, and the gradient of $\frac{N_{O^+}}{N_e}$ becomes steeper in the altitude range of 170 km–260 km. In particular, $\frac{N_{O^+}}{N_e}$ has a value of 0.6 at altitude ~215 km, 0.5 at altitude ~208 km, and 0.4 at altitude ~200 km, implying that O^+ dominates above altitude ~208 km, whereas $\frac{N_{(O_2^+ + NO^+)}}{N_e}$ behaves on the contrary and O_2^+ and NO^+ dominate below altitude ~208 km.

In summary, the altitude characteristics of the enhanced plasma line and ion line induced by PDI and OTSI show that (1) the altitude of the enhanced ion line and plasma line in the HB are lower than the altitude of the enhanced ion line and plasma line in the GB, (2) the enhanced ion line and plasma line are distributed within an extending altitude range, and (3) the altitude extension of the enhanced ion line occurs only in the HB, whereas the altitude extension of the enhanced plasma line occurs in both HB and GB.

3. Discussion

The Langmuir wave and ion acoustic wave enhanced by PDI and OTSI are observed by a radar in monostatic operation at the altitude where the Bragg condition is satisfied (Stubbe et al., 1992)

$$h = h_0 - \Delta h \tag{1}$$

where h_0 denotes the reflection altitude of the pump, $\Delta h = 12\frac{K_B f_r^2}{m_e c^2 f_{HF}^2} T_e H$, f_r is the radar frequency, m_e is the electron mass, c is the velocity of light, and H is the scale height. Obviously, Δh is dependent on T_e and H of plasma on the traveling path. For the sake of simplicity, considering the scale height of ~30 km to ~40 km for the typical ionosphere (Djuth et al., 1994), we can reasonably assume in this study that the reflection altitudes of the pump in the GB are approximately identical to the reflection altitudes of the pump in the HB, namely, $h_{0HB} \approx h_{0GB}$.

Further, H can be defined as (Liu et al., 2007)

$$\frac{1}{H} = -\frac{1}{N_e}\frac{dN_e}{dh} = \frac{m_i g}{K_B T_p} + \frac{m_i \nu_{in} W_D}{K_B T_p} + \frac{dT_p/dh}{T_p} \tag{2}$$

where m_i is the ion mass, g is the acceleration due to gravity, $T_p = \frac{T_i + T_e}{2}$ is the plasma temperature, ν_{in} is the collision frequency of ion with neutrals, and W_D is the vertical diffusion velocity of the ions.

Considering atomic oxygen as the most common ion species at the F_2 region and using $m_{iO^+} \approx 2.657 \times 10^{-26}$kg, $\nu_{in} \approx 4.1$Hz for the typical ionosphere (Rishbeth & Owen, 1969) and $W_D \approx 3.7$m/s (Wu et al., 2017), H and Δh can be obtained as shown in Table 1. Table 1 illustrates that the higher T_{e200} tends to increase H in the first, second, and fourth cycles. In the third cycle, however, H in the GB is somewhat larger than in the HB due to the enhanced temperature in the GB, showing that the higher electron temperature can make electrons overcome the gravity as well as the collisions more effectively and escape from the heated region, reshaping slightly the local altitude profile of the ionosphere. In addition, the higher T_{e200} tends to increase Δh in all four cycles. From the above discussions, the observing altitude should clearly be dependent essentially on the electron temperature; that is, a higher T_{e200} leads to a lower h.

However, the variations in altitude in the GB and HB in Table 1 are no greater than 1 km, whereas the variations in altitude in the GB and HB in Figures 1 and 2 are ~3 km. This error should be most likely caused by the model and the height resolution of the radar. Equation (1) was obtained by assuming the profile of the electron density $N_e(h) = N_e(h_0)\left(1 + \frac{h-h_0}{H}\right)$ rather than the real one (Stubbe et al., 1984, 1992). In addition, EISCAT UHF radar can give only the ion line and plasma line with the height resolution of ~3 km, which certainly results in the altitude ambiguity.

The most interesting aspect is that the enhanced ion line and plasma line are distributed within an extending altitude range. Furthermore, the altitude extension of enhanced ion line occurs only in the HB, whereas the altitude extension of enhanced plasma line occurs in the HB and GB. With regard to the field-aligned observation of the radar in monostatic operation, the enhanced Langmuir wave and ion acoustic wave traveling down in a nonuniform but stationary ionosphere will follow the dispersion functions (Kohl et al., 1993; Baumjohann and Treumann, 1997):

$$\omega_L^2 = \omega_{pe}^2 + \gamma\frac{K_B T_e}{m_e} k_L^2 \tag{3}$$

$$\omega_{ia}^2 = \gamma\frac{K_B T_e}{m_i} k_{ia}^2 \tag{4}$$

where ω_{pe} denotes the Langmuir frequency; k_L and k_{ia} are the wave numbers of the Langmuir wave and ion acoustic wave, respectively; m_i is an effective ion mass, and m_e is the electron mass. Based on the following approximations and assumptions, function (4) should be valid in the present study. (1) The ionospheric

Table 1
T_{e200}, H, and Δh During the Experiment[a]

	HB1	GB1	GB2	HB2	HB3	GB3	GB4	HB4
T_{e200}(K)	2,687	2,268	2,103	2,505	2,581	2,348	2,186	2,599
H(km)	46.85	41.56	39.38	44.33	44.33	45	41.63	46.6
Δh(km)	4.49	3.564	3.13	3.962	4.145	3.823	3.44	4.32

[a]The column headings denote the pump frequency bands and the heating cycles, e.g., HB1 for the HB in the first cycle.

plasma behaves quasi-neutral in the stationary state. (2) Due to $T_i << T_e$ in the F region, the contribution of ion thermal pressure is neglected, where T_i and T_e are the ion and electron temperature and have the means of 1,172.9 K and 2,212.5 K at altitude 214.4 km, respectively. (3) The excited ion acoustic wave travels in long wavelength or small wave number, namely, $k_{ia}^2\lambda_D^2 \approx 0.0006 << 1$, where $k_{ia} = \frac{2k_r}{2\pi} \approx 6.207\mathrm{m}^{-1}$, the Debye length $\lambda_D = \sqrt{\frac{\varepsilon_0 K_B T_e}{N_e e^2}} \approx 0.004\mathrm{m}$, and ε_0 is the vacuum dielectric constant, K_B is the Boltzmann constant, e is the electron charge, and N_e is the average electron density at altitude 214.4 km.

The dispersion function describes the relation between the wave and the medium. When the enhanced Langmuir wave and ion acoustic wave travel down in a nonuniform but stationary ionosphere, ω_L and ω_{ia} will not change, whereas k_L and k_{ia} may change. Furthermore, the change in k_L should depend on ω_{pe} and T_e, and the change in k_{ia} on m_i and T_e. In other words, ω_{pe} and T_e may be compensated by each other to keep k_L unchanged. Similarly, to keep k_{ia} unchanged, m_i and T_e may compensate each other.

Figure 4 shows that O^+ is dominant above altitude 208 km, whereas NO^+ and O_2^+ dominate over O^+ below altitude 208 km, implying that the term $\frac{1}{m_i}$ in equation ((4)) will decrease with the descent in altitude, namely, with a positive gradient. However, Figure 3 shows that the strong enhancement in T_e occurs at altitude ~200 km, where the upper hybrid resonance occurs (Dysthe et al., 1982; Gurevich et al., 1995; Mjølhus, 1993; Robinson et al., 1996; Wu et al., 2017). Unfortunately, however, one cannot see the morphology of T_e near altitude ~200 km due to the height resolution of ~15 km. Even so, surely, there should be a negative gradient of T_e above the upper hybrid resonance altitude; that is, T_e should become larger from the near altitude of 245.8 km to the upper hybrid resonance altitude. Thus, the gradient of T_e is obviously opposite to the gradient of $\frac{1}{m_i}$ above the upper hybrid resonance altitude. Similarly, the gradient of ω_{pe} in function (3) is opposite to that of T_e above the upper hybrid resonance altitude.

Figure 1 shows that ion acoustic waves in the HB can approximately satisfy the Bragg condition within the extending altitude range due to the competitive balance between the increasing m_i and T_e with the descent in altitude within the extending altitude range; that is, m_i and T_e may be compensated by each other so that $\frac{m_i}{T_e}$ and k_{ia} remain approximately unchanged within the extending altitude range. Thus, the altitude range examined may be covered by multiple range gates. In other words, the enhanced ion acoustic wave can be observed by UHF radar within the extending altitude range. Note that k_{ia} should satisfy the Bragg condition approximately rather than fully because the gradient of T_e is approximately equal to the gradient of m_i, albeit less fully. As an example, the enhanced ion line in the HB in the fourth cycle is examined. In Figure 5 (left), both m_i and $T_{e\mathrm{HB}}$ become larger with the descent in altitude above altitude 199.6 km. Figure 5 (right) shows that $k_{ia\mathrm{HB}}$ has a value of ~37 m^{-1} above altitude 199.6 km and becomes larger with the descent in altitude below altitude 199.6 km. Moreover, $\frac{dk_{ia\mathrm{HB}}}{dh}\Big|_{229.8\ \mathrm{km}}^{245.8\ \mathrm{km}} \approx 0.029\mathrm{m}^{-1}\mathrm{km}^{-1}$, $\frac{dk_{ia\mathrm{HB}}}{dh}\Big|_{214.4\ \mathrm{km}}^{229.8\ \mathrm{km}} \approx 0.008\mathrm{m}^{-1}\mathrm{km}^{-1}$, $\frac{dk_{ia\mathrm{HB}}}{dh}\Big|_{199.6\ \mathrm{km}}^{214.4\ \mathrm{km}} \approx -0.028\mathrm{m}^{-1}\mathrm{km}^{-1}$, and $\frac{dk_{ia\mathrm{HB}}}{dh}\Big|_{186.2\ \mathrm{km}}^{199.6\ \mathrm{km}} \approx -0.48\mathrm{m}^{-1}\mathrm{km}^{-1}$. This implies that $k_{ia\mathrm{HB}}$ remains unchanged approximately and is very close to $2k_r$ above altitude 199.6 km, satisfying the Bragg condition approximately above altitude 199.6 km. Thus, the enhanced ion acoustic wave can be observed in the altitude range of 199.6 km to 245.8 km.

Thus, a question arises. Why does the enhanced ion line in the GB not occur within an extending altitude range but at a particular altitude, as illustrated in Figure 1? As shown in Figure 3, when f_{HF} lies in the GB, the enhancement in T_e at altitude ~200 km is ~10% and far smaller than the enhancements in T_e in the HB and LB due to the absence of the trapping of the upper hybrid wave in the small-scale irregularities (Borisova et al., 2014, 2016; Dysthe et al., 1982; Gurevich et al., 1995; Mjølhus, 1993; Robinson et al., 1996; Wu et al., 2017). Thus, we can assume reasonably and approximately that T_e has not been modified by the

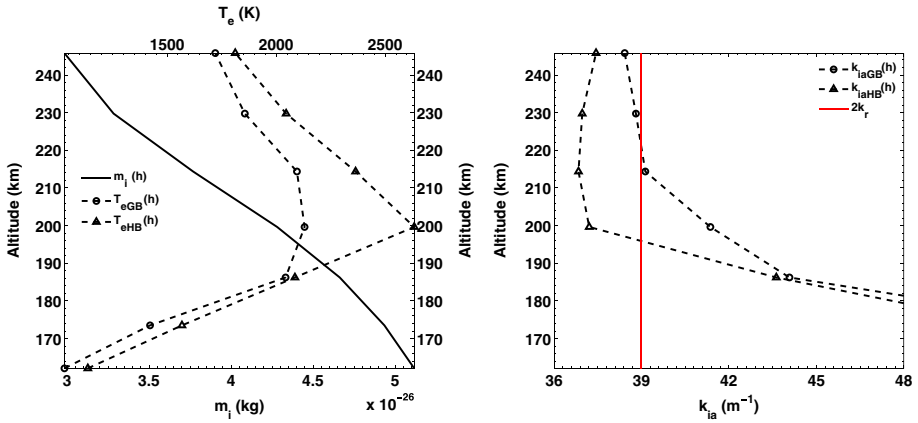

Figure 5. The profiles of (left) m_i, T_{e}GB, and T_{e}HB and (right) k_{ia}GB and k_{ia}HB within the altitude range of 162.1 km–245.8 km in the fourth cycle, where m_i is the effective ion mass; T_{e}GB and T_{e}HB are the average electron temperature in the GB and HB, respectively; and k_{ia}GB and k_{ia}HB are the wave numbers of the ion acoustic wave in the GB and HB. $m_i = \frac{N_{O^+}}{N_e} m_{iO^+} + \left(1 - \frac{N_{O^+}}{N_e}\right) m_{iO_2^+}$, $m_{iO^+} = 2.657\times10^{-26}$kg, and $m_{iO_2^+} = 5.314\times10^{-26}$kg. Due to $m_{iO_2^+} \approx m_{iNO^+}$, only $m_{iO_2^+}$ is utilized here. T_{e}GB is the mean of the electron temperature within the internal of [14:07:20 UT, 14:09:10 UT] and T_{e}HB within the internal of [14:11:20 UT, 14:18:00 UT]. The frequency of the ion acoustic wave f_{ia} = 9.45 kHz.

pump in the GB and can be considered a constant rather than a variable within the altitude range examined. In this case, k_{ia} in dispersion functions (4) will be determined only by m_i. In other words, k_{ia} will depend only on the altitude profile of m_i. Due to the monotonicity of the altitude profile of m_i, k_{ia} should satisfy the Bragg condition fully and inevitably at a specific altitude rather than within an extending altitude range. This specific altitude can be covered by only one range gate of radar. Similarly, the enhanced ion line in the GB in the fourth cycle is examined. Figure 5 (left) also illustrates that the average electron temperature in the GB T_{e}GB is enhanced slightly and is far smaller than the average electron temperature in the HB above altitude 199.6 km. Moreover, $\frac{T_{e\mathrm{GB}}}{dh}\Big|_{186.2\mathrm{km}}^{199.6\mathrm{km}} \approx 6.09\mathrm{Kkm}^{-1}$, $\frac{T_{e\mathrm{GB}}}{dh}\Big|_{199.2\mathrm{km}}^{214.4\mathrm{km}} \approx -2.36\mathrm{Kkm}^{-1}$, $\frac{T_{e\mathrm{GB}}}{dh}\Big|_{214.4\mathrm{km}}^{245.8\mathrm{km}} \approx -15.52\mathrm{Kkm}^{-1}$, $\frac{T_{e\mathrm{HB}}}{dh}\Big|_{186.2\mathrm{km}}^{199.6\mathrm{km}} \approx 40.82\mathrm{km}^{-1}$, $\frac{T_{e\mathrm{HB}}}{dh}\Big|_{199.2\mathrm{km}}^{214.4\mathrm{km}} \approx -18.45\mathrm{Kkm}^{-1}$, and $\frac{T_{e\mathrm{HB}}}{dh}\Big|_{214.4\mathrm{km}}^{245.8\mathrm{km}} \approx -20.65\mathrm{Kkm}^{-1}$. Thus, T_{e}GB can be considered the constant approximately above an altitude 199.6 km, and k_{ia}GB should be dominated by the profile of m_i, as expected from function (4). In Figure 5 (right), k_{ia}GB has a value of ~39 m^{-1} and remains unchanged approximately in the altitude range of 214.4 km to 245.8 km, namely, $\frac{dk_{ia\mathrm{GB}}}{dh}\Big|_{214.4\ \mathrm{km}}^{245.8\mathrm{km}} \approx -0.018\mathrm{m}^{-1}\mathrm{km}^{-1}$. Below altitude 214.4 km, however, k_{ia}GB becomes larger with the descent in altitude, that is, $\frac{dk_{ia\mathrm{GB}}}{dh}\Big|_{199.6\ \mathrm{km}}^{214.4\ \mathrm{km}} \approx -0.159\mathrm{m}^{-1}\mathrm{km}^{-1}$. Thus, k_{ia}HB is approximately equal to $2k_r$ and satisfies the Bragg condition approximately in the wide altitude range near altitude 214.4 km. In particular, k_{ia}GB = $39\mathrm{m}^{-1}$ at altitude 214.4 km, where the enhanced ion acoustic wave will certainly be observed.

The profile of k_{ia}HB is obviously dependent on the profiles of m_i and T_{e}HB above the altitude 199.6 km, whereas it is mainly dependent on the profile of m_i below the altitude 199.6 km, which is also true for k_{ia}GB. With the comparisons between Figure 5 (right) and Figure 1, however, some errors of the extending altitude range are obvious. The extending altitude ranges in Figure 5 (right) reach ~45 km and ~31 km in the HB and GB, respectively, whereas Figure 1 indicates that the extending altitude range is ~8.8 km in the HB and ~3 km in the GB. Those errors may be in two aspects, namely, the uncertainty in the altitude profile of the effective ion mass and the ambiguity in the altitude profile of electron temperature. In the GB, $\frac{dT_{e\mathrm{GB}}}{dh}$ is small; thus, the larger $\frac{dm_i}{dh}$ is necessary for the larger $\frac{dk_{ia\mathrm{GB}}}{dh}$. Considering a larger $\frac{dm_i}{dh}$ above 199.6 km, thus, k_{ia}GB above 212.5 km may become smaller and deviate greatly from 39 m^{-1}, whereas k_{ia}GB below 212.5 km will become larger and also deviate greatly from 39 m^{-1}. This implies that the extending altitude range in the GB will be compressed greatly. In the HB, however, the ambiguity in the altitude profile of electron temperature may play an important role. Assuming a smooth altitude profile of the effective ion mass as presented in Figure 1 (left) and considering a larger $\frac{dT_{e\mathrm{HB}}}{dh}$ above 199.6 km, thus, k_{ia}HB may become larger and deviate greatly from 39 m^{-1} above altitude 209.57 km. On the other hand, assuming a smooth altitude profile of electron temperature as presented in Figure 1 (left) and considering a larger $\frac{dm_i}{dh}$ above 199.6 km, thus, k_{ia}HB may become smaller and deviate greatly from 39 m^{-1} above altitude 209.57 km. The above two considerations

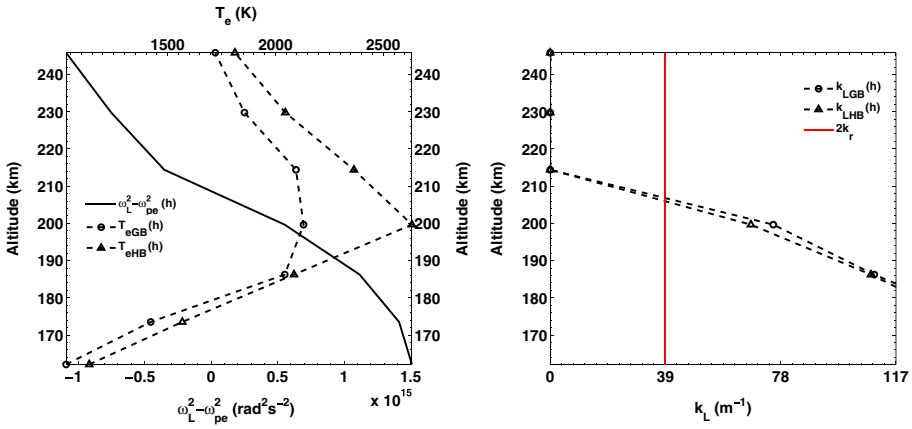

Figure 6. The same as Figure 5 but for the Langmuir wave, where $\omega_L = 2\pi \times 6.8$MHz, $\omega_{pe} = 2\pi \times 8.9\sqrt{N_e}$, N_e is the mean of electron density within the internal of [14:07:20 UT, 14:09:10 UT], and $k_{L\mathrm{GB}}$ and $k_{L\mathrm{HB}}$ are the wave numbers of the Langmuir wave in the GB and HB, respectively.

in the HB imply that the upper boundary of the extending altitude range will descend; that is, the extending altitude range in the HB will be compressed greatly.

Thus, it may be seriously questioned whether the uncertainty in the altitude profile of the effective ion mass or the ambiguity in the altitude profile of electron temperature dominates those errors in this study. As the above discussions, if a smooth altitude profile of the effective ion mass is assumed, a larger $\frac{dT_{e\mathrm{HB}}}{dh}$ above 199.6 km will lead to a larger $k_{ia\mathrm{HB}}$ deviating greatly from 39 m^{-1} above altitude 209.57 km. Then $k_{ia\mathrm{HB}}$ should be exactly equal to 39 m^{-1} at altitudes 209.57 km or 206.63 km, so that the intensity in ion line at altitudes 209.57 km or 206.63 km should be strong and up to ~1. However, Figure 1 shows that the intensity in the enhanced ion line in the HB is up to ~0.85. Thus, it seems that those errors are dominated by the uncertainty in the altitude profile of the effective ion mass. Indeed, $\frac{dm_i}{dh}$ is eventually dependent on the ion density gradients in different species.

Moreover, the extending altitude of ~3 km to ~5 km of the normalized ion line power is contributed to the virtual observation at a frequency of 933 MHz/2 (Kohl et al., 1993; Stubbe et al., 1992). Based on the above discussions, however, an alternative explanation is that the altitude extension of ~3 km to ~5 km may be due to the mutual compensation between T_e and m_i on the traveling path, although the altitude profiles of T_e and m_i were not given by Stubbe et al. (1992) and Kohl et al. (1993). Additionally, there is also a stronger ion line power higher up between the altitudes of the UHF and VHF plasma lines (Kohl et al., 1993; Stubbe et al., 1992). Strictly, it is not necessary for the real ionosphere that the enhanced ion acoustic wave and Langmuir wave are observed at the same altitude, because the dispersion relation of the Langmuir wave is different from the dispersion relation of the ion acoustic wave; that is, the change in k_L is dependent on ω_{pe} and T_e on the traveling path, whereas the change in k_{ia} is on T_e and m_i. In other words, at a specific altitude where the Langmuir wave satisfies the Bragg condition, the ion acoustic wave does not necessarily satisfy the Bragg condition, and vice versa.

Figure 2 shows that the enhanced plasma line is also distributed within an extending altitude range. Unlike the enhanced ion line, the altitude of the enhanced plasma line is extending not only in the HB but also in the GB, implying that k_L in the GB and HB can satisfy the radar Bragg condition within the extending altitude range. Due to the competitive balance between the increasing $\omega_L^2 - \omega_{pe}^2$ and the increasing T_e with the descent in altitude, $\omega_L^2 - \omega_{pe}^2$ and T_e may be compensated by each other so that k_L satisfies the Bragg condition and remains unchanged within the extending altitude range, which may be covered by multiple range gates. Thus, the enhanced Langmuir wave can be observed by UHF radar in the extending altitude range. Figure 6 (left) illustrates the profiles of $\omega_L^2 - \omega_{pe}^2$, $T_{e\mathrm{GB}}$, and $T_{e\mathrm{HB}}$. Similar to m_i, $\omega_L^2 - \omega_{pe}^2$ trends up with the descent in altitude, namely, with a negative gradient. Moreover, one can see that $\omega_L^2 - \omega_{pe}^2$ becomes negative above altitude 208.5 km. This is dependent on the profile of N_e; that is, ω_{pe} is larger than ω_L above altitude 208.5 km, where the Langmuir wave should reflect. Correspondingly, in Figure 6 (right), the profiles of $k_{L\mathrm{GB}}$ and $k_{L\mathrm{HB}}$ above altitude 208.8 km should be zero. In Figure 6 (right), $k_{L\mathrm{GB}}$ and $k_{L\mathrm{HB}}$ are equal to 39 m^{-1} at

altitudes of ~207 km and ~206 km, respectively, and the profiles of $k_{L\mathrm{GB}}$ and $k_{L\mathrm{HB}}$ almost coincide within the altitude range examined. Moreover, $\frac{dk_{L\mathrm{GB}}}{dh}\Big|_{199.6\mathrm{km}}^{214.4\mathrm{km}} \approx -5.1\mathrm{m}^{-1}\mathrm{km}^{-1}$, $\frac{dk_{L\mathrm{GB}}}{dh}\Big|_{186.2.6\mathrm{km}}^{199.6\mathrm{km}} \approx -2.46\mathrm{m}^{-1}\mathrm{km}^{-1}$, $\frac{dk_{L\mathrm{HB}}}{dh}\Big|_{199.6\mathrm{km}}^{214.4\mathrm{km}} \approx -4.59\mathrm{m}^{-1}\mathrm{km}^{-1}$, and $\frac{dk_{L\mathrm{HB}}}{dh}\Big|_{186.2.6\mathrm{km}}^{199.6\mathrm{km}} \approx -3.03\mathrm{m}^{-1}\mathrm{km}^{-1}$; that is, $k_{L\mathrm{GB}}$ and $k_{L\mathrm{HB}}$ should satisfy the Bragg condition approximately within the narrow altitude range near the altitudes of ~207 km and ~206 km. Considering the height resolution of ~3 km, the enhanced Langmuir wave should be observed in the altitude range of ~203 km to ~210 km. As an altitude function, however, the profiles of $T_{e\mathrm{GB}}$ and $T_{e\mathrm{HB}}$ do not vary monotonically within the altitude range of 162.1 km to 245.8 km, whereas $\omega_L^2 - \omega_{pe}^2$ trends up monotonically with the descent in altitude. This implies that in our case, $\omega_L^2 - \omega_{pe}^2$ should dominate $k_{L\mathrm{GB}}$ and $k_{L\mathrm{HB}}$; that is, the altitude extension of the enhanced plasma line in the GB and HB is dependent mainly on the profile of N_e, although the altitude extension is not independent of the profile of T_e as expected from function (3).

A typical experimental result is that a narrow altitude extension of the plasma line always accompanies a wide altitude extension of the ion line (Kohl et al., 1993; Stubbe et al., 1992). Analogous to our result, although it is not independent of the profile of the electron temperature, the altitude extension of the enhanced plasma line is dependent mainly on the profile of the electron density, whereas the altitude extension of the enhanced ion line is dominated by the profiles of ion mass and electron temperature, which may obviously be compensated by each other.

Even so, this analysis will not contradict that the profile of the enhanced T_e may lead to the altitude extension of the enhanced plasma line. Considering a small gradient profile of N_e, the profile of T_e may dominate k_L; that is, k_L will be dependent on the profile of T_e when N_e is a constant approximately within the altitude range examined, as should be expected from equation (3). This may be supported by some other measurements. The measurements acquired during an ionospheric heating campaign conducted in November 1990 show that the enhanced plasma turbulence plunges downward in altitude over timescales of tens of seconds following the HF beam turn on, exhibiting billowing, cloudlike structures, thereafter recovering slightly toward greater altitudes (Djuth et al., 1994, see plate 1). At the initial stage of evolution of 0.5 ± 5 s, T_e will not be enhanced greatly at the upper hybrid resonance altitude due to the undeveloped small-scale irregularity and less anomalous absorption (Gurevich, 2007). Then, k_L will depend only on the altitude profile of the electron density and satisfy the Bragg condition fully and inevitably at a particular altitude, where the narrow power profile of the plasma line was observed as shown in the literature (Djuth et al., 1994, see plate 1). Thereafter, the small-scale irregularities at the upper hybrid resonance altitude begin to govern anomalous absorption of the pump gradually with increasing time, so T_e at the upper hybrid resonance altitude will be enhanced greatly. Further, the thermal energy should be conducted within an extending altitude range near the upper hybrid resonance altitude. Then, k_L will depend not only on the altitude profile of the electron density but also on the altitude profile of T_e, satisfying the Bragg condition approximately within an extending altitude range. Moreover, the altitude interval becomes lower and lower due to the gradual enhancement in T_e, as expected from equation (1), and wider and wider due to the thermal conduction along the magnetic field. After ~30 s of the pump onset, the diffusion of the plasma along the magnetic field may lead to the decrease in the local electron density, which is equivalent to the decrease in H and Δh. Additionally, the diffusion of plasma induced by a long pump pulse of ~30 s may slightly reshape the altitude profile of the electron density (M. T. Rietveld, private communication). Then, the reflection altitude of the pump may move upward. As a result, a new heating region should be obtained at a greater altitude.

It should be stressed that the profiles of $\omega_L^2 - \omega_{pe}^2$, $T_{e\mathrm{GB}}$, and $T_{e\mathrm{HB}}$ were taken from the measurement of UHF radar. Comparing Figure 6 (right) with Figure 2, the profiles of $k_{L\mathrm{GB}}$ and $k_{L\mathrm{HB}}$ can match perfectly the observing altitudes of the plasma lines in the GB and HB in the fourth cycle, thus showing indirectly that the model $m_i = \frac{N_{O^+}}{N_e} m_{iO^+} + \left(1 - \frac{N_{O^+}}{N_e}\right) m_{iO_2^+}$ may lead to the errors of the extending altitude range of the enhanced ion line as shown in Figure 5 (right).

4. Conclusions

This paper focuses on the altitude characteristics of the enhanced ion line and the plasma line during an ionospheric heating campaign with a pump frequency near the fifth gyroharmonic on 11 March 2014 at the EISCAT Tromsø site in northern Norway. Those UHF observations show that the observing altitude of the

enhanced ion line and plasma line varies as a function of pump frequency. The observing altitude of the enhanced ion line and plasma line in the HB is lower than the observing altitude of the enhanced ion line and plasma line in the GB. The enhanced ion lines in the HB are distributed within an extending altitude range, whereas the enhanced ion lines in the GB are observed at a specific altitude. Moreover, the enhanced plasma lines in the HB and GB are distributed within an extending altitude range.

In conclusion, the altitude characteristic of the enhanced plasma line and ion line are brought about essentially by the thermal effect induced by the heating. (1) The altitude of the enhanced ion line and plasma line is determined by the electron temperature and the scale height. (2) In the HB, ion mass and electron temperature may be compensated by each other so that the wave number of ion acoustic wave remains unchanged and satisfies the Bragg condition approximately within the extending altitude range. (3) Due to a slight enhancement in the electron temperature in the GB, the wave number of the ion acoustic wave will depend mainly on the profile of the ion mass and will satisfy the Bragg condition at a particular altitude. (4) The altitude extension of the enhanced plasma line in the GB and HB is dependent mainly on the profile of the electron density, although they are not independent of the profile of the electron temperature. Even so, the enhanced electron temperature may lead to the altitude extension of the plasma line by considering a small gradient profile of electron density.

This study may provide an alternative explanation for the altitude extension of the enhanced ion line and plasma line during ionospheric heating. Furthermore, an alternative clue for the explanation of an "overshoot" in the plasma line and ion line occurs when the heating switching is on initially (Djuth et al., 1994; Kohl et al., 1993; Showen & Kim, 1978) may be expected.

Acknowledgments
We would like to thank the engineers of EISCAT in Tromsø for keeping the facility in excellent working condition and the Tromsø Geophysical Observatory, UiT, the Arctic University of Norway, for providing the magnetic data of Tromsø recorded on 11 March 2014. The data from the UHF radar can be obtained freely from EISCAT (http://www.eiscat.se/schedule/schedule.cgi). The EISCAT Scientific Association is supported by China (China Research Institute of Radiowave Propagation), Finland (Suomen Akatemia of Finland), Japan (the National Institute of Polar Research of Japan and Institute for Space-Earth Environmental Research at Nagoya University), Norway (Norges Forkningsrad of Norway), Sweden (the Swedish Research Council), and the UK (the Natural Environment Research Council).

References

Ashrafi, M., Kosch, M. J., & Honary, F. (2006). Heater-induced altitude descent of the EISCAT UHF ion line enhancements: Observations and modeling. *Advances in Space Research*, *38*(11), 2645–2652. https://doi.org/10.1016/j.asr.2005.06.079

Baumjohann, W., & Treumann, R. A. (1997). *Basic space plasma physics*. London: Imperial College Press.

Bezzerides, B., & Weinstock, J. (1972). Nonlinear saturation of parametric instabilities. *Physical Review Letters*, *28*(8), 481–484. https://doi.org/10.1103/PhysRevLett.28.481

Bilitza, D., & Reinisch, B. W. (2008). International Reference Ionosphere 2007: Improvements and new parameters. *Advances in Space Research*, *42*(4), 599–609. https://doi.org/10.1016/j.asr.2007.07.048

Blagoveshchenskaya, N. F., Borisova, T. D., Kosch, M., Sergienko, T., Brändström, U., Yeoman, T. K., & Häggström, I. (2014). Optical and ionospheric phenomena at EISCAT under continuous X-mode HF pumping. *Journal of Geophysical Research: Space Physics*, *119*, 10,483–10,498. https://doi.org/10.1002/2014JA020658

Borisova, T. D., Blagoveshchenskaya, N. F., Kalishin, A. S., Kosch, M., Senior, A., Rietveld, M. T., … Hagstrom, I. (2014). Phenomena in the high-latitude ionospheric F region induced by a HF heater wave at frequencies near the fourth electron gyroharmonic. *Radiophysics and Quantum Electronics*, *57*(1), 1–19. https://doi.org/10.1007/s11141-014-9489-6

Borisova, T. D., Blagoveshchenskaya, N. F., Kalishin, A. S., Rietveld, M. T., Yeoman, T. K., & Hagstrom, I. (2016). Modification of the high-latitude ionospheric F region by high-power HF radio waves at frequencies near the fifth and sixth electron gyroharmonics. *Radiophysics and Quantum Electronics*, *58*(8), 561–585. https://doi.org/10.1007/s11141-016-9629-2

Carlson, H. C., Gordon, W. E., & Showen, R. L. (1972). High frequency induced enhancements of the incoherent scatter spectrum at Arecibo. *Journal of Geophysical Research*, *77*, 1242–1250. https://doi.org/10.1029/JA077i007p01242

Chen, H. C., & Fejer, J. A. (1975). Saturation spectrum of the parametric decay instability in the presence of an external magnetic field. *Physics of Fluids*, *18*(12), 1809. https://doi.org/10.1063/1.861062

Cheng, M., Xu, B., Wu, Z., Li, H., Wang, Z., Xu, Z., … Wu, J. (2013). Observation of VHF incoherent scatter spectra disturbed by HF heating. *Journal of Atmospheric and Terrestrial Physics*, *105-106*, 245–252. https://doi.org/10.1016/j.jastp.2013.08.010

Cheung, P. Y., Dubois, D. F., Fukuchi, T., Kawan, K., Rose, H. A., Russell, D. F., … Wong, A. Y. (1992). Investigation of strong Langmuir turbulence in ionospheric modification. *Journal of Geophysical Research*, *97*, 10,575–10,600. https://doi.org/10.1029/92JA00645

Cheung, P. Y., Sulzer, M. P., DuBois, D. F., & Russell, D. A. (2001). High-power high-frequency-induced Langmuir turbulence in the smooth ionosphere at Arecibo. II. Low duty cycle, altitude-resolved, observations. *Physics of Plasmas*, *8*(3), 802–812. https://doi.org/10.1063/1.1345704

Djuth, F. T., & DuBois, D. F. (2015). Temporal development of HF-excited Langmuir and ion turbulence at Arecibo. *Earth, Moon, and Planets*, *116*(1), 19–53. https://doi.org/10.1007/s11038-015-9458-x

Djuth, F. T., Stubbe, P., Kohl, H. W., Rietveld, M. T., & Elder, J. H. (1994). Altitude characteristics of plasma turbulence excited with the Tromsø Superheater. *Journal of Geophysical Research*, *99*, 333–339.

Drake, J. F., Lee, Y. C., Schmid, G., Liu, C. S., & Rosenbluth, M. N. (1974). Parametric instabilities of electromagnetic waves in plasmas. *Physics of Fluids*, *17*(4), 778. https://doi.org/10.1063/1.1694789

DuBois, D. F., & Goldman, M. V. (1965). Radiation induced in stability of electron plasma oscillations. *Physical Review Letters*, *14*(14), 544–546. https://doi.org/10.1103/PhysRevLett.14.544

DuBois, D. F., & Goldman, M. V. (1967). Parametrically excited plasma fluctuations. *Physics Review*, *164*(1), 207–222. https://doi.org/10.1103/PhysRev.164.207

Dubois, D. F., & Goldman, M. V. (1972). Nonlinear saturation of parametric instability: Basic theory and application to the ionosphere. *Physics of Fluids*, *15*(5), 919. https://doi.org/10.1063/1.1694000

Dubois, D. F., Rose, H., & Russell, D. (1988). Power spectra of fluctuations in strong Langmuir turbulence. *Physical Review Letters*, *61*(19), 2209–2212. https://doi.org/10.1103/PhysRevLett.61.2209

Dubois, D. F., Rose, H., & Russell, D. (1990). Excitation of strong Langmuir turbulence in plasmas near critical density: Application to HF heating of the ionosphere. *Journal of Geophysical Research*, *95*, 21,221–21,272. https://doi.org/10.1029/JA095iA12p21221

Dubois, D. F., Rose, H., & Russell, D. (1991). Coexistence of parametric decay cascades and caviton collapse at subcritical densities. *Physical Review Letters*, *66*(15), 1970–1973. https://doi.org/10.1103/PhysRevLett.66.1970

Dubois, D. F., Hanssen, A., Rose, H. A., & Russell, D. (1993a). Space and time distribution of HF excited Langmuir turbulence in the ionosphere: Comparison of theory and experiment. *Journal of Geophysical Research*, *98*, 17,543–17,567. https://doi.org/10.1029/93JA01469

DuBois, D. F., Hansen, A., Rose, H. A., & Russell, D. (1993b). Excitation of strong Langmuir turbulence in the ionosphere: Comparison of theory and observations. *Physics of Fluids B: Plasma Physics*, *5*(7), 2616–2622. https://doi.org/10.1063/1.860699

DuBois, D. F., Russell, D. A., Cheung, P. Y., & Sulzer, M. P. (2001). High-power high-frequency-induced Langmuir turbulence in the smooth ionosphere at Arecibo. I. Theoretical predictions for altitude-resolved plasma line radar spectra. *Physics of Plasmas*, *8*(3), 791–801. https://doi.org/10.1063/1.1345703

Dysthe, K. B., Mjølhus, E., Pécseli, H., & Rypdal, K. (1982). Thermal cavitons. *Physica Scripta*, *T2/2*, 548.

Fejer, J. A. (1979). Ionospheric modification and parametric instabilities. *Reviews of Geophysics*, *17*, 135–153. https://doi.org/10.1029/RG017i001p00135

Gordon, W. E., & Carlson, H. C. (1974). Arecibo heating experiments. *Radio Science*, *9*, 1041–1047. https://doi.org/10.1029/RS009i011p01041

Gurevich, A. V. (2007). Nonlinear effects in the ionosphere. *Physics Uspekhi*, *50*(11), 1091–1121. https://doi.org/10.1070/PU2007v050n11ABEH006212

Gurevich, A. V., Zybin, K. P., & Lukyanov, A. V. (1995). Stationary striations developed in the ionospheric modification. *Physical Review Letters*, *75*(13), 2622–2625. https://doi.org/10.1103/PhysRevLett.75.2622

Hagfors, T., Kofman, W., Kopka, H., & Stubbe, P. (1983). Observations of enhanced plasma lines by EISCAT during heating experiments. *Radio Science*, *18*, 861–866. https://doi.org/10.1029/RS018i006p00861

Jones, T. B., Robinson, T. R., Stubbe, P., & Kopka, H. (1986). EISCAT observations of the heated ionosphere. *Journal of Atmospheric and Terrestrial Physics*, *48*(9-10), 1027–1035. https://doi.org/10.1016/0021-9169(86)90074-7

Kantor, I. J. (1974). High frequency induced enhancements of the incoherent scatter spectrum at Arecibo. II. *Journal of Geophysical Research*, *79*, 199–208.

Kohl, H. W., Kopka, H., Lahoz, C., & Stubbe, P. (1987). Propagation of artificially excited Langmuir waves in the ionosphere. *Radio Science*, *22*, 655–661. https://doi.org/10.1029/RS022i004p00655

Kohl, H., Kopka, H., Stubbe, P., & Rietveld, M. T. (1993). Introduction to ionospheric heating experiments at Tromso-II. Scientific problems. *Journal of Atmospheric and Terrestrial Physics*, *55*(4-5), 601–613. https://doi.org/10.1016/0021-9169(93)90008-M

Kuo, S. P., & Cheo, B. R. (1978). Parametric excitation of coupled plasma waves. *Physics of Fluids*, *21*(10), 1753. https://doi.org/10.1063/1.862091

Kuo, Y. Y., & Fejer, J. A. (1972). Spectral-line structures of saturated parametric instabilities. *Physical Review Letters*, *29*(25), 1667–1670. https://doi.org/10.1103/PhysRevLett.29.1667

Lehtinen, M., & Huuskonen, A. (1996). General incoherent scatter analysis and GUISDAP. *Journal of Atmospheric and Terrestrial Physics*, *58*(1-4), 435–452. https://doi.org/10.1016/0021-9169(95)00047-X

Liu, L., Le, H., Wan, W., Sulzer, M. P., Lei, J., & Zhang, M. (2007). An analysis of the scale heights in the lower topside ionosphere based on the Arecibo incoherent scatter radar measurements. *Journal of Geophysical Research*, *112*, A06307. https://doi.org/10.1029/2007JA012250

Mjølhus, E. (1993). On the small scale striation effect in ionospheric radio modification experiments near harmonics of the electron gyro frequency. *Journal of Atmospheric and Terrestrial Physics*, *55*(6), 907–918. https://doi.org/10.1016/0021-9169(93)90030-3

Nordling, J., Hedberg, A., Wannberg, G., Leyser, T. B., Derblom, H., Opgenoorth, H. J., & Lahoz, C. (1988). Simultaneous bistatic European Incoherent Scatter UHF, 145–MHz radar and stimulated electromagnetic emission observations during HF ionospheric modification. *Radio Science*, *23*(5), 809–819. https://doi.org/10.1029/RS023i005p00809

Perkins, F. W., & Flick, J. (1971). Parametric instabilities in inhomogeneous plasmas. *Physics of Fluids*, *14*(9), 2012. https://doi.org/10.1063/1.1693711

Perkins, F. W., Oberman, C., & Valeo, E. J. (1974). Parametric instabilities and ionospheric modification. *Journal of Geophysical Research*, *79*(10), 1478–1496. https://doi.org/10.1029/JA079i010p01478

Rietveld, M. T., Kohl, H., Kopka, H., & Stubbe, P. (1993). Introduction to ionospheric heating at Tromsø-I. Experimental overview. *Journal of Atmospheric and Terrestrial Physics*, *55*(4/5), 577.

Rietveld, M. T., Senior, A., Markkanen, J., & Westman, A. (2016). New capabilities of the upgraded EISCAT high-power HF facility. *Radio Science*, *51*, 1533–1546. https://doi.org/10.1002/2016RS006093

Rishbeth, H., & Owen, K. (1969). *Introduction to ionospheric physics*. New York: Academic Press.

Rishbeth, H., & Van Eyken, A. (1993). EISCAT: Early history and the first ten years of operation. *Journal of Atmospheric and Terrestrial Physics*, *55*(4-5), 525–542. https://doi.org/10.1016/0021-9169(93)90002-G

Robinson, T. R. (1989). The heating of the high latitude ionosphere by high power radio waves. *Physics Reports*, *179*(2-3), 79–209. https://doi.org/10.1016/0370-1573(89)90005-7

Robinson, T. R., Honary, F., Stocker, A. J., Jones, T. B., & Stubbe, P. (1996). First EISCAT observations of the modification of F-region electron temperatures during RF heating at harmonics of the electron gyro frequency. *Journal of Atmospheric and Terrestrial Physics*, *58*(1-4), 385–395. https://doi.org/10.1016/0021-9169(95)00043-7

Rosenbluth, M. N. (1972). Parametric instabilities in inhomogeneous media. *Physical Review Letters*, *29*(9), 565–567. https://doi.org/10.1103/PhysRevLett.29.565

Showen, R. L., & Kim, D. M. (1978). Time variations of HF–induced plasma waves. *Journal of Geophysical Research*, *83*(A2), 623. https://doi.org/10.1029/JA083iA02p00623

Silin, V. P. (1965). Parametric resonance in a plasma. *Soviet Physics – JETP (English Translation)*, *21*, 1127.

Stubbe, P., Kopka, H., Thide, B., & Derblom, H. (1984). Stimulated electromagnetic emission: A new technique to study the parametric decay instability in the ionosphere. *Journal of Geophysical Research*, *89*(A9), 7523–7536. https://doi.org/10.1029/JA089iA09p07523

Stubbe, P., Kopka, H., Rietveld, M. T., Frey, A. W., Hoeg, P., Kohl, H. W., & Holt, O. (1985). Ionospheric modification experiments with the Tromsø heating facility. *Journal of Atmospheric and Terrestrial Physics*, *47*(12), 1151–1163. https://doi.org/10.1016/0021-9169(85)90085-6

Stubbe, P., Kohl, H., & Rietveld, M. T. (1992). Langmuir turbulence and ionospheric modification. *Journal of Geophysical Research*, *97*(A5), 6285. https://doi.org/10.1029/91JA03047

Wang, X., Zhou, C., Liu, M., Honary, F., Ni, B., & Zhao, Z. (2016). Parametric instability induced by X–mode wave heating at EISCAT. *Journal of Geophysical Research: Space Physics*, *121*, 10,536–10,548. https://doi.org/10.1002/2016JA023070

Weinstock, J., & Bezzerides, B. (1972). Threshold of ionospheric modifications by radio waves. *Journal of Geophysical Research*, *77*(4), 761–764. https://doi.org/10.1029/JA077i004p00761

Wu, J., Wu, J., & Xue, Y. (2006). The effect of the production and loss reactions on the parametric instability. *International Journal of Computational Fluid Dynamics*, *20*(7), 491–496. https://doi.org/10.1080/10618560600909986

Wu, J., Wu, J., & La Hoz, C. (2007). On the ponderomotive force and the effect of loss reaction on parametric instability. *Chinese Physics*, *16*(2), 558.

Wu, J., Wu, J., & Xu, Z. (2016). Results of ionospheric heating experiments involving an enhancement in electron density in the high latitude ionosphere. *Plasma Science and Technology*, *18*(9), 890–896. https://doi.org/10.1088/1009-0630/18/9/03

Wu, J., Wu, J., Rietveld, M. T., Haggstrom, I., Zhao, H., & Xu, Z. (2017). The behavior of electron density and temperature during ionospheric heating near the fifth electron gyrofrequency. *Journal of Geophysical Research: Space Physics*, *122*(1), 1277–1295. https://doi.org/10.1002/2016JA023121